ArcticNet for Semantic Segmentation of Meltpond Regions in the Arctic Sea Ice

Aqsa Sultana, *Student Member, IEEE,* Vijayan K. Asari, *Senior Member, IEEE,* Ivan Sudakow and Lee W. Cooper

***Abstract*—As climate change drives global temperatures upward, seasonal sea ice in the Arctic is rapidly diminishing, leading to the formation of meltponds. Meltponds absorb more solar radiation compared to snow due to lower reflectivity (albedo), accelerating the melting of the ice underneath. The manual assessment of the complex boundaries of meltponds is a demanding and time-consuming endeavor. To streamline this process, we introduce a novel method for detecting and segmenting meltponds based on the UNet architecture, named ArcticNet. Our framework combines two UNets that incorporate recurrent, residual and attention operations. The first UNet extracts intermediate features that are further refined by the second UNet improving overall performance by learning hierarchical representations. The proposed architecture possesses the ability to enhance the boundaries of meltponds while accurately capturing their precise locations. The inclusion of residual and recurrent operations gives an expanded field of view for segmentation. Combining this with an attention gate, which concentrates primarily on target regions of diverse shapes and sizes, has been demonstrated to enhance the overall performance and robustness of the network by boosting model sensitivity and improving predictions. The performance of our model was assessed using 3–channel (RGB), high–resolution aerial images from Healy–Oden Trans Arctic Expedition (HOTRAX) and NASA's Operation IceBridge. The ArcticNet architecture categorized the HOTRAX and Operation IceBridge images into three and two classes respectively. HOTRAX include meltponds, open water, and snow, whereas Operation IceBridge includes only meltponds and snow. The new algorithm showed superior performance in segmenting meltponds when compared to other state-of-the-art approaches.**

***Index Terms*—Arctic Ocean, meltpond, WNet, residual, recurrent, UNet, R2UNet, attention gate, HOTRAX, Operation IceBridge.**

I. Introduction

THE earth's average temperature has rapidly increased over the past years in large part due to natural and human–made greenhouse gas emissions. The rise in temperatures has disproportionately impacted the Arctic, leading to accelerated sea ice melting and the formation of meltponds and disruption in Arctic ecosystems at rates that are unprecedented [1]. Meltponds are pools of water that appear on sea ice primarily due to the melting of snow on the sea ice surface in the summer. The formation and further development of these "windows" into the underlying ocean can affect energy balance and albedo [2], [3]. These pools of water reflect less sunlight compared to snow and absorb more solar radiation, accelerating the melting process and reinforcing the cycle of ice melting through a positive feedback loop [4], [5]. This positive feedback raises air temperatures during the freezing season, reducing the formation of new ice. Due to this, the summer melt season is lengthening, and winter ice growth is slowing, leading to more open water in the Arctic Ocean [4], [5]. This phenomenon makes meltponds a visual and measurable indicator and feeds into a positive feedback loop that accelerates Arctic warming. Their extent and characteristics provide direct evidence of changes in temperature and seasonal ice melt which are critical markers of climate change. Given the substantial impact of meltponds on accelerating sea ice loss, these features can serve as a valuable metric for quantifying the response of Arctic sea ice to global warming [6]. An automated approach to detect meltpond development and extent would be highly beneficial for environmental monitoring due to the localized and swiftly changing nature of these features [7]. Quantitative analyses and dynamics of meltpond size, shape, and distribution can provide valuable insights into their evolution over time by observing the area of meltponds at different times of the year for multiple years. These data are essential for monitoring changes in sea ice extent and for validating numerical models that simulate climate dynamics [8]. Manual monitoring of the formation and growth of meltponds using classical methods of image analysis and statistics is time-consuming. Automating a universal process by identifying boundaries around meltponds would enable more efficient calculation of crucial metrics, such as the transition from meltponds to open water [9]. The current study focuses on the extraction of meltpond regions by robust segmentation methods on images captured in one season. The main goal is to develop deep learning techniques for robust meltpond detection based on CNN segmentation methods. Ultimately, accurate segmentation contributes to the ability to predict future sea ice conditions and to develop effective strategies to mitigate climate change, as well as to understand contributions to climate change at high latitudes [1].

Various techniques are employed for segmentation of the Arctic region, including traditional image processing methods

This work is supported by the division of physics at the National Science Foundation (NSF), Grant No. 2102906. (*Corresponding author: Vijayan K. Asari, e-mail: vasari1@udayton.edu*).

Aqsa Sultana and Vijayan K. Asari are with the Vision Lab and Dept. of Electrical and Computer Engineering, University of Dayton, Dayton, Ohio 45469, USA (e-mail: sultanaa3@udayton.edu; vasari1@udayton.edu).

Ivan Sudakow is with the School of Mathematics and Statistics, The Open University, Milton Keynes, MK7 6AA, U.K (e-mail: ivan.sudakow@open.ac.uk).

Lee W. Cooper is with the Center for Environmental Science, University of Maryland, Solomons, Maryland, 20688, USA (e-mail: cooper@umces.edu).

The HOTRAX Dataset is available at https://zenodo.org/records/6602409#.Yqkm9XbMJPY. The Operation IceBridge dataset is available at https://forms.gle/SJRvqci1tCrZ8Miu5. Information about the original IceBridge Data is available at https://icebridge.gsfc.nasa.gov/?page_id=732.

like thresholding and edge detection [10], [11], as well as more advanced deep learning-based approaches such as the well-known UNet based architectures where it automatically learns and extracts hierarchical features from the data reducing the need for manual feature annotation. These models, in addition to their ability to leverage existing datasets to learn distinctive features, can also perform segmentation and classification simultaneously. This capability is particularly important for detecting meltponds as they share the same microwave signature as open water making them challenging to detect. The similarity in microwave signatures causes meltponds to obscure the ice beneath them, creating the illusion of less ice than is actually present [12], [13]. Therefore, to validate the effectiveness of proposed models on identifying meltponds, we utilize a dataset that contains satellite and airborne imagery [12] that features meltponds as pools of water in the Arctic [14]. This paper examines applications of UNet and its architectural variations, along with our proposed method, ArcticNet, specifically targeting the boundaries surrounding meltponds and similar regions. Through testing and evaluation, the new model, ArcticNet demonstrates enhanced and superior performance compared to UNet, R2UNet, WNet.

Our main contributions include:

- We propose a novel model for semantic segmentation of the Arctic region: ArcticNet, combining the strengths of UNet, R2UNet, WNet and an attention mechanism.
- The novel architecture consists of two parallel networks (1) A Dual-Network Structure where the first network extracts hierarchical features and propagates them effectively to the second network via skip connections. The second network refines these features, ensuring enhanced boundary detection and accurate segmentation. (2) Utilization of the skip connection from the decoder of the first UNet to the encoder of the second UNet for the easy propagation of the hierarchical features (3) Recurrent operation and residual connection in the block continuously looking back at the features and propagating changes from input to output respectively (4) Adding an attention mechanism to ArcticNet weights the features that are essential for producing boundaries, focusing primarily on the foreground rather than the background.
- The effectiveness of the proposed segmentation models is validated using the high–resolution, RGB images from HOTRAX and NASA's Operation IceBridge datasets.

By focusing on features critical for boundary delineation, ArcticNet is aimed at improving the accuracy of meltpond segmentation by capturing complex shapes found in HOTRAX and NASA's Operation IceBridge datasets.

II. Literature Review

Background: Meltponds form during the spring-summer melt season when the meltwater on the surface collects in the local depressions, evolving from small, rounded pools to irregular, connected networks as melt and drainage progress. During the initial stages of sea ice melt, it is common for meltwater to pool over the underlying ice surface [15]. The appearance of these meltponds alter light transmission and albedo and can increase primary production in the underlying water column due to the reduced albedo associated with meltponds [16]. The reduced albedo increases shortwave absorption relative to snow and bare ice [15], [17]. On relatively smooth first-year ice (FYI), ponds tend to be shallower and laterally extensive; on rougher multiyear ice (MYI), ponds are typically deeper and more segmented, constrained by hummocks and ridges [18],[19], [20]. Modeling of meltpond evolution on MYI indicates meltponds can persist slightly longer than on FYI [20]. However, the proportion of MYI in the Arctic Ocean has been in sharp decline in recent decades [21]. Thus, the differences in the evolution and spatial extent of meltponds on MYI relative to FYI may be becoming less and less consequential.

Meltpond Physical, Morphological, and Radiative Properties (by sea-ice type): Ponds initiate once meltwater from snow and surface ice accumulates in microtopographic lows. Over the season, isolated circular ponds coalesce into branching networks as drainage pathways open. Snow depth/distribution, freeboard, permeability thresholds, and roughness (ridges, hummocks) govern planform geometry, area–perimeter scaling, and depth—properties that modulate lateral ablation and light transmission [18], [19], [20]. FYI's smoother topography favors laterally continuous, shallow ponds and often higher peak pond fractions; once permeability increases, drainage can be abrupt. MYI tends to host deeper, more segmented ponds constrained by hummocky relief and lower early-season permeability [17], [18], [19], [20]. For segmentation, FYI scenes often present broad, low-contrast water–ice boundaries, whereas MYI scenes present fragmented, high-curvature pond edges. Ponds reduce albedo and increase shortwave absorption relative to snow/bare ice, enhancing melt and increasing light transmission to the upper ocean [17], [22], [23]. Transient conditions complicate both physics and detection: (i) fresh snowfall can blanket ponds and collapse optical contrast; (ii) thin overnight skim-ice brightens and textures surfaces; and (iii) wind roughening alters both optical bidirectional reflectance distribution function (BRDF) and radar backscatter. During refreezing, snow can preferentially accumulate on refrozen ponds and reduce their light transmittance below that of adjacent bare ice [24]. These behaviors motivate robustness tests and targeted data augmentation in learning-based segmentation.

SAR Imagery: In optical (VIS/NIR) imagery, ponds appear dark/blue against bright snow/ice, enabling spectral/unmixing approaches to estimate pond fraction when skies are clear [25], [26]. However, fresh snowfall and thin overnight "skim-ice" can temporarily brighten ponds and suppress contrast. In SAR, calm ponds are radar-dark, but wind roughening introduces centimetric capillary–gravity waves that markedly increase X-/C-band backscatter; thin refreezing and wet snow can further brighten surfaces [27], [28], [29]. Single- or dual-polarization X-band pond retrievals are sensitive to surface state. Modest winds roughen pond water and brighten returns; thin refreezing or wet snow increases backscatter further, reducing separability from rough ice. Studies mitigate this with polarization ratios and texture features, yet accuracy degrades under windy/refreeze conditions. While somewhat

similar features can appear on glacial ice, the use of image processing methods we explore here is restricted to sea ice surfaces. In this paper, our experiments and evaluations are focused entirely on optical imagery.

Image Processing Methods: Otsu's method [30] is an image processing technique applied to analyze meltpond configurations. By utilizing aerial images of Arctic sea ice from the surface heat budget of the Arctic Ocean (SHEBA) and HOTRAX databases, this approach developed an algorithmic framework for mapping meltpond configurations onto graphs of nodes and edges. This method demonstrated the extraction of valuable structural information about meltponds. A limitation to note is that the estimated conductivity factor was merely correlated with the permeability or conductivity of the meltpond network, which underlined the need for further research to clarify this relationship. The thresholding method [31] explored the quantification of daily changes in fractional meltpond and snow cover. Using a time series of photographic infrared imagery collected from a tethered balloon at an altitude of 300 meters during the Seasonal Sea Ice Monitoring and Modelling Site (SIMMS) experiment in 1995, this method allowed the tracking of meltpond dynamics over short timescales. However, setting constant threshold values across the time series images was a challenge due to invariant light conditions, and during the early melt season, the network could not distinguish melt features from wet snow and accurately segment the regions in the images. A third study combined different spectral bands to investigate the possibility of obtaining meltpond fraction estimates [32]. This method leveraged ENVISAT WSM images with HH-polarization focused on detecting open water and meltponds. By combining bands, the study enhanced the ability to discern subtle variations in spectral responses which led to more accurate mapping of surface features. Lastly, the use of image processing software, such as ENVI@EX [33], demonstrated the effectiveness of synthetic aperture radar (SAR) systems in meltpond studies. Helicopter-based airborne SAR surveys conducted in the northern Chukchi Sea during the summer of 2011 were employed to map meltponds and derive detailed information on their fraction, size, and shape.

Machine Learning Methods: The Maximum Likelihood Method [34] utilized aerial photographs collected during helicopter flights as part of the CHINARE2010 expedition. This technique was applied to classify meltponds, open water, and snow-covered ice, which primarily focused on evaluating the spatial variability of these features. It was able to synthesize information on small-scale sea ice features that satellite data often missed; however, it was unable to address the spatial and temporal coverage in the aerial observations of sea ice and meltponds. Another study explored decision tree and random forest models based on polarimetric parameters [29], which utilized TerraSAR-X dual-polarization data and airborne SAR images. The primary objective was to develop an approach to retrieve meltpond statistics using advanced polarimetric data. The study highlighted the robustness of these methods in deriving accurate statistics and improving the detection of meltponds from high-resolution SAR datasets. However, due to its limited spatial resolution of the TerraSAR-X data compared to airborne SAR, it was unable to estimate the number density of ponds accurately and the mean of the pond area, which prevented the detection of smaller meltponds. Multilayer perceptron model based on spectral curve differences [25] analyzed moderate resolution imaging spectroradiometer (MODIS) data, A level-3 MODIS surface-reflectance data with aerial photographs from the 2008 MELTEX campaign in the Beaufort Sea and with National Snow and Ice Data Center (NSIDC) observations from four distributed Arctic sites collected in 2000 and 2001. This study aimed to quantify surface fractions of meltponds, open water, and snow and ice across the entire Arctic region. Since it simplified complex Arctic sea ice cover into a three-surface-class model, surface types like thin ice were misclassified, and it also led to uncertainties in fractional coverage estimates. Furthermore, the integration of a multilayer neural network with multinomial logistic regression [35] demonstrated a robust framework for pan-Arctic meltpond classification. Using MODIS data from 2001 to 2019 and combining statistical and machine learning approaches, it achieved significant advancements in binary classification tasks for remote sensing applications.

Deep Learning Methods: Semantic segmentation using convolutional neural networks (CNNs) has gained significant attention in recent years due to its effectiveness in various computer vision tasks, such as image segmentation and object recognition. Current segmentation models follow encoder-decoder architecture. A brief literature review highlighting the key works in this area is presented here. UNet, a CNN based architecture was designed in 2015. It emerged as a leading solution for pixel-level classification in medical image analysis, subsequently extending its applicability to various other domains owing to its remarkable success rate. The objective was to perform hierarchical feature propagation allowing it to capture both high-level and low-level contexts with skip connections in encoder-decoder manner [36]. DeepLab, Atrous Convolution, and Fully Connected Conditional Random Fields (CRFs) were introduced in 2016 achieving state-of-the-art performance on various segmentation benchmarks. The semantic segmentation task was performed by applying the atrous convolution with upsampled filters to control the resolution at which the feature responses by enlarging the field of view. It was further extended to atrous spatial pyramid pooling (ASPP) to segment objects in multiple scales. The outputs were combined with fully connected CRFs for robust localization [37]. In the same year, Pyramid Scene Parsing Network (PSP Net) was introduced by leveraging a pyramid pooling module to capture contextual information at multiple scales to achieve robust semantic segmentation results [38]. In 2017, WNet introduced the concept of parallel architectures which was built by combining two fully convolutional networks into an encoder-decoder framework, with each Fully Connected Network (FCN) being a variant of the UNet architecture [39]. In 2018, Attention UNet was introduced by adding attention gates (AGs) to focus on target structures of different shapes and sizes by suppressing irrelevant information while enhancing salient features. AGs were added to the decoding unit of the UNet instead of skip connections to increase the model sensitivity [40]. In the same year, Recurrent Residual UNet (R2UNet)

was introduced by incorporating recurrent operation for feature accumulation obtained by feedback loop and residual learning for feature propagation in encoding and decoding units of UNet for medical image segmentation achieving state-of-the-art performance [41]. In 2019, EfficientNet was introduced for model scaling by balancing network depth, width and resolution using an efficient compound coefficient. The approach effectively scaled up MobileNets and ResNet models [42].

In 2021, Attention R2UNet was introduced which utilized the strength of R2UNet and attention mechanisms for multi-modal medical image segmentation. R2AUNet replaced the original skip connections with attention gates [43]. AMB-WNet was introduced in 2022 by embedding attention gates in multi-bridge WNet to suppress irrelevant background areas. It comprised of a down-sample group, an up-sample group, a central block which was a novel inverted U-shaped module, and a connection group that integrated attention gates and multi-scale convolution [44].

UNet's symmetric encoder-decoder with skip connections excelled in fast, data-efficient medical and remote sensing segmentation, but its reliance on local convolutions and transpose-convolution upsampling missed global context and introduced checkerboard artifacts. R2UNet was built on UNet by incorporating residual and recurrent blocks that deepened feature reuse and enlarged the effective receptive field. It increased the accuracy in fine structures, but it inflated parameters and training time. Adding attention gates to UNet focused the decoder on salient encoder features by sharpening boundary delineation and mitigating class-imbalance drift, though at the cost of extra memory and slower inference, while R2AUNet had the same benefits with the richer R2 feature flow, it produced state-of-the-art detail retention but it risked overfitting on small datasets, became computationally bulky and prone to noise due to the nested residual–recurrent operation. WNet's two stacked UNets refined outputs in a coarse-to-fine cascade that captured hierarchical context and smooth predictions, but the doubled architecture increased the GPU demands, increased redundant feature learning, and in the absence of dedicated attention or residual mechanisms, it struggled to capture extremely small or sparsely represented objects.

In this paper, we propose ArcticNet as a means for pixel-level multi-class segmentation of imagery sourced from HOTRAX and Operation IceBridge. The new model utilizes the strength of recurrent neural network for repetitive refinement, residual learning for feature transmission from input to the output, two UNets in "W" shape for coarse-to-fine conversion that captures hierarchical feature context, skip connection from decoding unit of the first UNet to the encoding unit of the second UNet for the feature propagation forming a shape of an "A" and an attention mechanism to capture modular dependencies by increasing the model sensitivity. The model follows the structure of WNet and R2UNet frameworks, which are based on UNet. The architectural details, experimental setup, results, discussion and conclusions are discussed in the sections below.

III. Proposed Model Architecture

ArcticNet is an integrated convolutional neural network that combines and extends the design principles of UNet [36], R2UNet [41], and WNet [39]. It preserves the encoder–decoder symmetry of UNet while adopting the residual and recurrent refinement strategy from R2UNet to enhance feature reuse and stabilize gradient flow. ArcticNet inherits the dual-UNet coarse-to-fine hierarchy of WNet, allowing hierarchical context aggregation and improved boundary localization. In addition to these inherited elements, ArcticNet, introduces two major componants: (1) a cross-network skip connection linking the decoder of the first network to the encoder of the second, which facilitates propagation of semantically rich features for hierarchical refinement, and (2) additive attention gates that adaptively weight spatial features to emphasize meltpond boundaries while suppressing background noise. These integrated modifications yield more precise pixel-wise segmentation and improved robustness in delineating meltpond, snow, and open water regions, as illustrated in Fig. 1.

The architecture adopts a "W" shape in which twin UNets with attention modules in the decoding paths, as shown in Fig. 2, are arranged in a sequential manner [39], [45]. Each UNet [36] is structured with a contracting path, known as the encoding unit, consisting of CNN blocks with 3×3 convolution. Recurrent connections between corresponding layers in the encoding unit enable the retention of information from previous steps, thereby enhancing its ability to accumulate features by repetitive refinement similar to R2UNet [41], [46], [47]. However, for ArcticNet, we used $t = 1$ as greater time periods induce significant instability issues for deep networks [48], [49], especially within networks that utilize attention gates. Additionally, residual connections [50] are integrated within each block to facilitate gradient flow, mitigating the vanishing gradient issue during training and also for feature transmission from input to the output. These connections enable the model to learn residual mappings, which contributes to more stable and efficient training [51]. The output of the Recurrent Residual Convolutional Neural Network (RRCNN as shown in Fig. 3 (a)) undergoes down-sampling via a 2×2 max-pooling operation after batch normalization where feature maps are doubled in number, and their sizes reduced in half. Concatenation is applied to map the low-level features from the encoding units to decoding units in the sequentially arranged UNet. Both UNets have their encoding units connected to the decoding units via a bridge [45].

The recurrent convolutional layer (RCL) builds with discrete time steps t as seen in Fig. 3 (b). Therefore, output of the RRCNNs at a center pixel of an input at (a, b) can be formulated mathematically as:

$$O^{a,b}(t) = (w^{a,b})^f(t) * x_i^{a,b}(t) + (w^{a,b})^r(t-1) * (x_i^{a,b})^r(t-1). \quad (1)$$

Here, for the standard neural convolutional layers and RCL, $(w^{a,b})^f(t)$ and $(w^{a,b})^r(t-1)$ are the weights respectively, and the terms $x_i^{a,b}(t)$ and $(x_i^{a,b})^r(t-1)$ are the inputs respectively. The output of the recurrent convolutional block, $O^{a,b}(t)$,

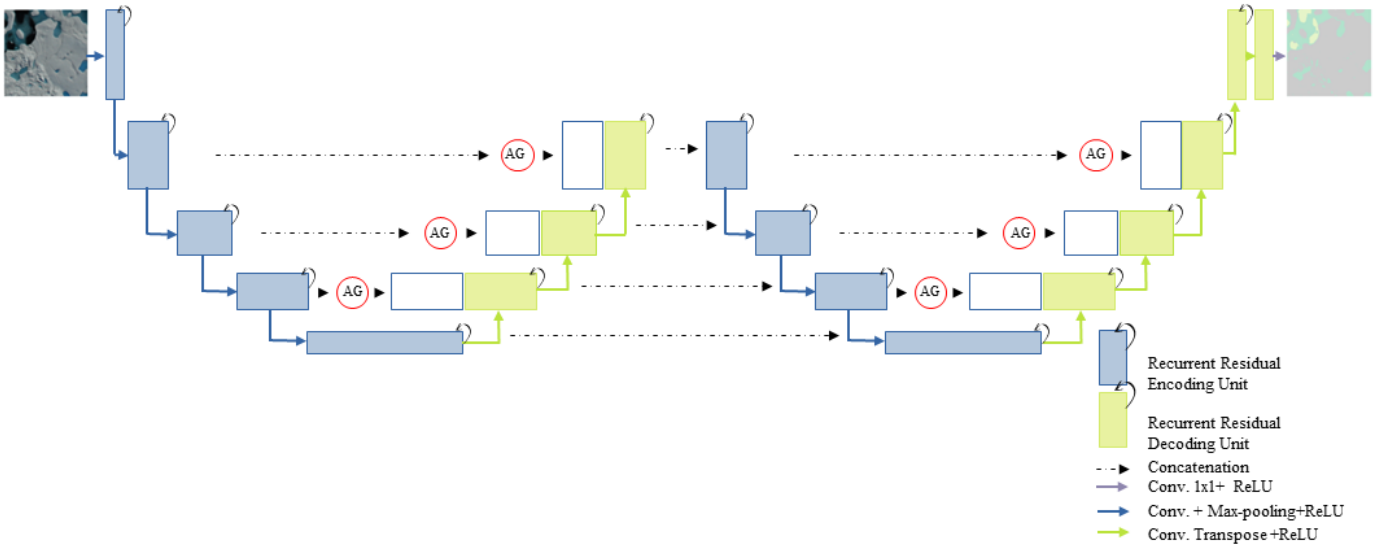

Fig. 1. ArcticNet architecture with the recurrent operation for repetitive refinement, residual learning for feature transmission, self-attention mechanism to capture modular dependencies and feature propagation from the decoding unit of the first UNet to the encoding unit of the second UNet of the WNet framework.

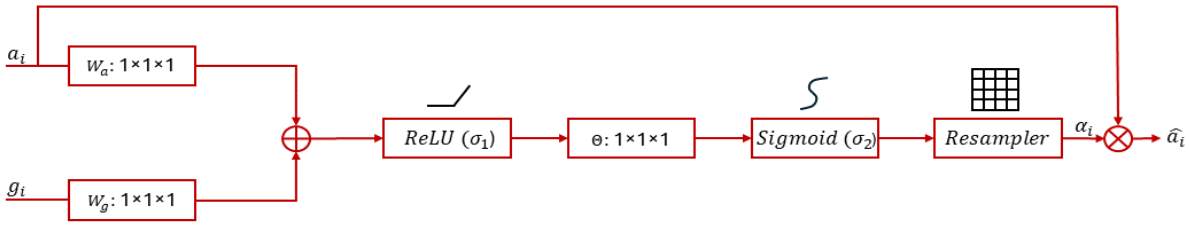

Fig. 2. Additive attention gate of ArcticNet in which the input features a_i are scaled by attention coefficients α_i. The attention coefficients are produced by trilinearly interpolated grid resampling of the sum of linearly transformed input features a_i and gating signal g_i.

which is generated from the above mathematical process, is then fed to the ReLU activation function and is defined as:

$$O^{a,b}(t) = f[O^{a,b}(t)] = max(0, O^{a,b}(t)). \quad (2)$$

The final output in the block is obtained after integrating with the residual unit and it can be calculated as follows:

$$x_{i+1}^{a,b}(t) = x_i^{a,b}(t) + O^{a,b}(t). \quad (3)$$

The term $x_{i+1}^{a,b}(t)$ represents the output of RRCNN block at time step t as shown in Fig 3 (a). The output is used for the immediate subsampling and upsampling processes in the decoding unit and encoding unit respectively [41], [52], [53].

In the decoding unit, each block performs an up-sampling operation where the size of the image is increased, and the number of feature maps is decreased. The decoding units of the first UNet are concatenated with the corresponding encoding units of the second UNet for feature accumulation, residual refinement of features in a hierarchical manner, and learning more complex and abstract representations of the data [45]. The final layer performs a 1×1 convolutional operation by

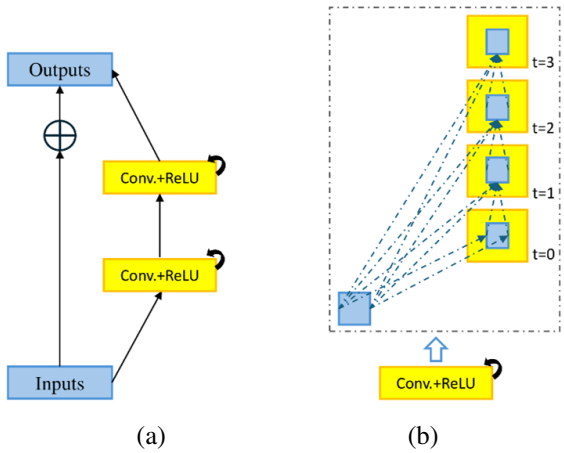

Fig. 3. Recurrent Residual Convolution Unit (RRCU) from encoding unit and decoding unit of ArcticNet (a) Recurrent Residual Convolutional Layer (RRCL); (b) Unfolded RRCL with $t = 3$.

restoring it to the original image and matching the desired number of classes. The final layer uses a softmax activation

function, which converts a vector of a certain number of real numbers into a probability distribution of possible outcomes.

ArcticNet employs attention gates which are incorporated into the decoding units of both the UNets to dynamically weigh the importance of various spatial locations or feature maps to capture modular dependencies within the network. The output of a batch normalization and transpose layer is fed into the attention gate to recalibrate the output features generated by the encoder. This occurs before merging them with the corresponding features in the decoder at each resolution. This enables the model to selectively focus on relevant image regions while suppressing irrelevant (background) or noisy information [54], thereby enhancing overall performance and interpretability [43].

Additive attention is applied to each pixel in the image where a_i and g_i are features from encoding unit and decoding unit at position i. The term g_i, gating signal, is also determined as a per-pixel focus area, allowing for contextualization of low-level information. The terms, σ_1 and σ_2 are ReLU and sigmoid activation functions respectively. W_a, W_g, b_g and b_θ are learnable parameter matrices (weight matrices) and bias terms respectively [43]. The attention gate is described as C_{att} and is defined below as:

$$C_{att} = \theta(\sigma_1(W_a a_i + W_g g_i + b_g)) + b_\theta. \tag{4}$$

$$\alpha_i = \sigma_2(C_{att}). \tag{5}$$

The attention scores are calculated by applying a linear transformation of a $1 \times 1 \times 1$ convolution to the concatenated features of the input tensors by using a sigmoid activation. The re-sampler is calculated with trilinear interpolation in contrast to other methods for achieving attention coefficients α_i (Eq. 5) to interpolate values from a grid based on the attention scores. This entire attention gate process is illustrated in Fig. 2. This approach allows for more spatially sensitive attention coefficients, as the interpolation considers neighboring values in the grid to compute the final attention coefficients for each position in the input tensors. The output $\hat{a}_i$ of the attention gate is element-wise multiplication of input feature maps as shown in Fig. 2 [40] and defined in Eq. 6.

$$\hat{a_i} = \alpha_i \times a_i. \tag{6}$$

IV. Experimental Setup and Results

Training was conducted using two Titan RTX GPUs. The code utilized TensorFlow's [55] GPU acceleration to take advantage of the data parallelization available with the dual GPU setup. This method accelerates learning as it allows for processing on both GPUs, which is particularly beneficial for handling large datasets and complex models. The average training time was 2 hours for 100 epochs. The Keras [56] open library framework was chosen for experimentation, leveraging its compatibility with TensorFlow and other backend engines. We used 128GB RAM and an Intel Core i9-9820X CPU.

A. Dataset

For evaluation of all the models, we used high resolution images from the following two datasets:

1) HOTRAX: The aerial dataset includes the morphological and optical characteristics of summer Arctic sea ice cover during the Healy Oden TRans Arctic EXpedition (HOTRAX) captured covering the Arctic Basin transect from 76 2.119N 157 55.807 W to 80 28.254 N 7 34.4 E [57], [58]. A Nikon D70 digital camera mounted on a helicopter captured aerial imagery between August 12th and September 26th, 2005, as part of HOTRAX. The captured images had dimensions of $3042 \times 2048 \times 3$ pixels with a spatial resolution of 5-25 cm/pixel depending on the altitude as the flights were flown at different altitudes of 150–700 m to avoid clouds. One hundred images of three classes consisting of meltponds, open water, and snow regions were selected for the experiments from the total set of 1013 images captured during this expedition. These images underwent visual analysis and manual annotations leading to the creation of three distinct categories. Figure 4 shows some image samples from the HOTRAX dataset [12], [59], [60].

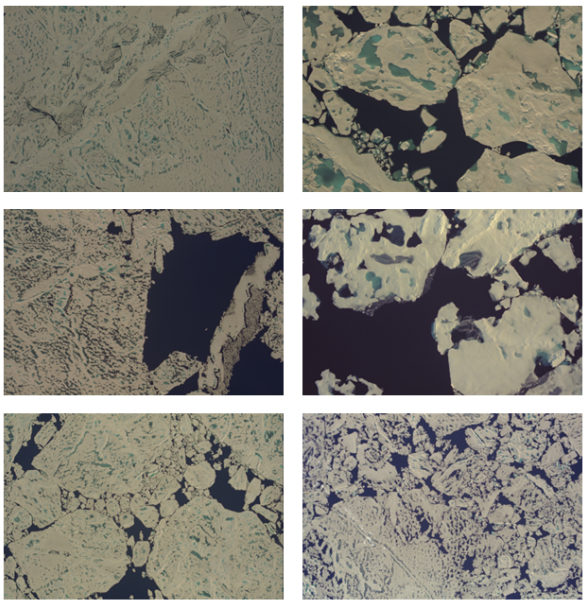

Fig. 4. HOTRAX high-resolution aerial images acquired during a joint US-Swedish icebreaker cruise across the Arctic Ocean in 2005.

2) NASA's Operation IceBridge: The IceBridge dataset [61] contains Level 1B imagery obtained from the Digital Mapping System (DMS) within NASA's Operation IceBridge from 16 October 2009 to 19 April 2018 with spatial coverage: N:-53S:-90E:180W:-180, N:90S:60E:180W:-180. The collected images were captured as part of Operation IceBridge funded aircraft survey campaigns. The current dataset is the collection of 536 Level 1B images captured in July 2016 during flights over the Chukchi Sea. The imagery has a spatial resolution of 10 cm with dimensions varying around $5500 \times 3500 \times 3$ pixels. The 170 images of 536 available were manually assessed and classified into two classes: meltponds and snow on sea ice. Sample images are shown in Fig. 5. [62].

B. Training Method

All the models were trained using ADAM optimizer with a learning rate set to 1×10^{-4} and a batch size of 2. A

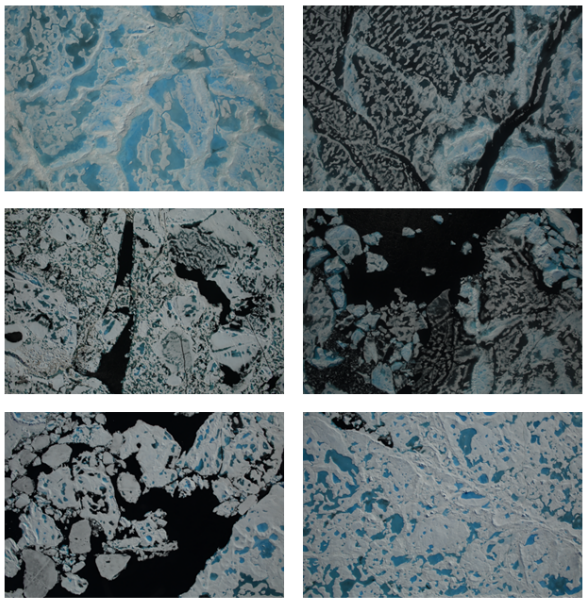

Fig. 5. Geolocated and orthorectified high-resolution images from NASA's Operation IceBridge campaign across the Arctic Ocean conducted between 2009-2020.

categorical loss and softmax activation function were used for the loss function and the final layer activation function, respectively. The data labels are transformed into one-hot encoded matrix where an integer class vector is converted into a binary class matrix. The model configuration was adjusted to produce better performance based on the specific requirements such as time step for recurrent operations and model depth which are identified during the tweaking/tuning process. The time step $t = 3$ was used for evaluating R2UNet and $t = 1$ was used for ArcticNet due to model depth. For Operation IceBridge images, we created a dataset of image patches with the dimension $1000 \times 1000 \times 3$ of 120, 30, 20 images for training, validation and testing respectively. The patch size of the HOTRAX dataset was $1200 \times 800 \times 3$ and the number of images in training, validation and testing included 60, 25 and 15 images respectively.

C. Quantitative Analysis

TABLE I
TRAINING AND TESTING TIME OF ARCTICNET, WNET, R2UNET AND UNET FOR 100 EPOCHS.

Model	Operation IceBridge		HOTRAX	
	Training (seconds)	Testing	Training (seconds)	Testing
UNet	**1700**	**5**	**1600**	**5**
R2UNet	3900	5	3100	5
WNet	3200	4	2500	4
ArcticNet	4300	8	4400	10

Table I compares the overall training and testing times in seconds for the four models: ArcticNet, WNet, R2UNet, and UNet. The models are evaluated over two datasets, Operation IceBridge and HOTRAX each trained for 100 epochs. The UNet model consumes the least training time for both Operation IceBridge and HOTRAX datasets, taking 1700 and 1600 seconds, respectively, with a testing time of 5 seconds. Conversely, ArcticNet has the longest training time of 4300 seconds for Operation IceBridge and 4400 seconds for HOTRAX with the highest testing times of 8 and 10 seconds respectively. WNet balances out UNet and ArcticNet with the training times of 3200 seconds on Operation Icebridge and 2500 seconds on HOTRAX, while having the fastest testing times of 4 seconds for both. R2UNet falls in the middle range for training, with 3900 seconds on Operation Icebridge and 3100 seconds on HOTRAX, with a testing duration of 5 seconds. The variation in training and testing times across Operation IceBridge and HOTRAX is largely influenced by each model's architectural complexity and the characteristics of the datasets. ArcticNet exhibits the longest training durations because its network design is deep, and more complex due to skip connections, attention blocks, and recurrent and residual operations used for feature extraction, requiring heavier computational overhead. By comparison, UNet uses a more straightforward encoder-decoder structure with fewer parameters, resulting in significantly faster training. The varying sizes, resolutions, and complexities of the Operation IceBridge and HOTRAX datasets also contribute to the training and testing durations. Larger or more diverse images can demand more computational resources and time for highly complex models.

All models underwent evaluation using the test data to compare their effectiveness and robustness in establishing meltpond boundaries across various regions within the two high-resolution Arctic datasets. Table II and Table III present the evaluation results for UNet, R2UNet, WNet and ArcticNet on HOTRAX and Operation IceBridge respectively. We also conducted experiments on ArcticNet without the attention mechanism (ArcticNet$^-$) to study the impact of the attention mechanism on the ArcticNet model.

The quantitative comparison of UNet, R2UNet, WNet, ArcticNet$^-$ and ArcticNet on the HOTRAX dataset shows that ArcticNet achieves the best overall performance, with the highest F1 score of 0.919, accuracy of 96.39%, precision of 0.933, recall of 0.903, and mean Intersection over Union (mIoU) of 0.854. ArcticNet$^-$, which excludes the attention mechanism, also performs strongly, achieving an F1 score of 0.909, accuracy of 96.01%, and mIoU of 0.838, indicating the significant contribution of the attention mechanism to ArcticNet's final performance. It also emphasizes the impact of hierarchical, semantically rich feature propagation from decoders of the first UNet to the corresponding encoders of the second UNet by scoring the second highest when compared with WNet, R2UNet and UNet. WNet follows in performance, with an F1 score of 0.912, accuracy of 95.33%, and an mIoU of 0.809, demonstrating robust but slightly lower effectiveness. R2UNet performs moderately well, with an F1 score of 0.889, accuracy of 95.26%, and an mIoU of 0.808, while UNet shows the lowest scores, including an F1 score of 0.883 and an mIoU of 0.798. This comparison highlights ArcticNet's superior performance in segmentation tasks.

The performance gain among the models highlights ArcticNet's superiority in segmentation tasks. Compared to UNet,

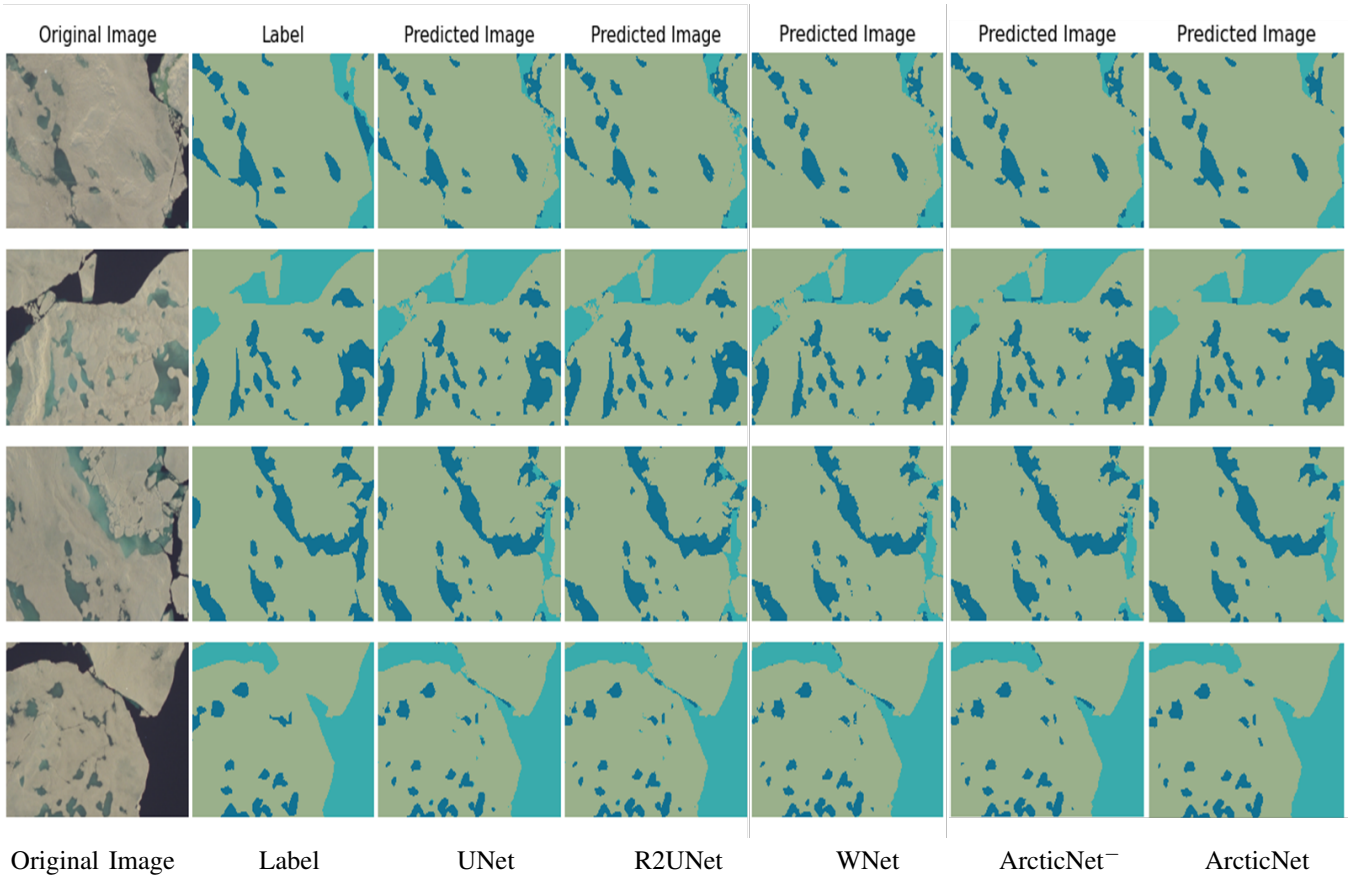

Fig. 6. Segmented outputs on HOTRAX dataset. Left to right: Original image, Ground Truth label, and predicted segmentations by UNet, R2UNet, WNet, ArcticNet$^-$ and ArcticNet.
Legends: Open water, Meltpond, Snow.

ArcticNet shows a significant improvement in mIoU, increasing from 0.798 to 0.854, which represents a 7.0% relative gain. Similarly, ArcticNet improves over R2UNet and WNet, with mIoU gains of 5.7% and 5.6%, respectively. The inclusion of the attention mechanism also provides a notable improvement over ArcticNet$^-$, with a relative mIoU gain of 1.9

TABLE II
QUANTITATIVE PERFORMANCE COMPARISON OF UNET, R2UNET, WNET, ARCTICNET$^-$ (ARCTICNET WITHOUT ATTENTION MECHANISM) AND ARCTICNET (WITH ATTENTION MECHANISM) EVALUATED ON HOTRAX DATASET.

	F1	ACC	PR	RE	mIOU
UNet	0.883	94.99%	0.884	0.882	0.798
R2UNet	0.889	95.26%	0.896	0.883	0.808
WNet	0.912	95.33%	0.907	0.876	0.809
ArcticNet$^-$	0.909	96.01%	0.927	0.893	0.838
ArcticNet	**0.919**	**96.39%**	**0.933**	**0.903**	**0.854**

The quantitative comparison on the Operation IceBridge dataset demonstrates that ArcticNet achieves the best performance across all metrics. It records the highest F1 score of 0.969, accuracy of 97.85%, precision of 0.983, recall of 0.957, and mIoU of 0.941. ArcticNet$^-$ also performs competitively, achieving an F1 score of 0.962, accuracy of 97.35%, and mIoU of 0.928, further illustrating the benefit of the attention mechanism in enhancing segmentation outcomes. WNet and R2UNet follow closely, with comparable performance; WNet achieves an mIoU of 0.918 and R2UNet scores 0.917, both demonstrating strong segmentation capabilities. UNet shows the lowest performance, with an F1 score of 0.938 and an mIoU of 0.885. Overall, ArcticNet's substantial improvements in accuracy, precision, and mIoU highlight its effectiveness and robustness in segmentation tasks on this dataset.

The performance gain on the Operation IceBridge dataset highlights ArcticNet's advancements over earlier models. Compared to UNet, ArcticNet achieves a substantial mIoU improvement from 0.885 to 0.941, reflecting a 6.3% relative gain. It also improves over R2UNet and WNet, with relative mIoU gains of 2.6% and 2.5%, respectively. Moreover, ArcticNet shows a 1.4% relative mIoU gain over ArcticNet$^-$ reinforcing the effectiveness of incorporating the attention mechanism into the architecture. These gains underscore ArcticNet's superior performance in accurately and robustly segmenting data in the Operation IceBridge dataset.

The enhancements acquired in ArcticNet due to attention gate's adaptive feature-weighting indication improvements reduce noise and emphasize relevant features. Better contextual understanding is achieved by aggregating contextual information from different parts of the input data and improving model interpretability [63]. In addition, the integration of recurrent and residual learning contributes to increased robustness and accuracy.

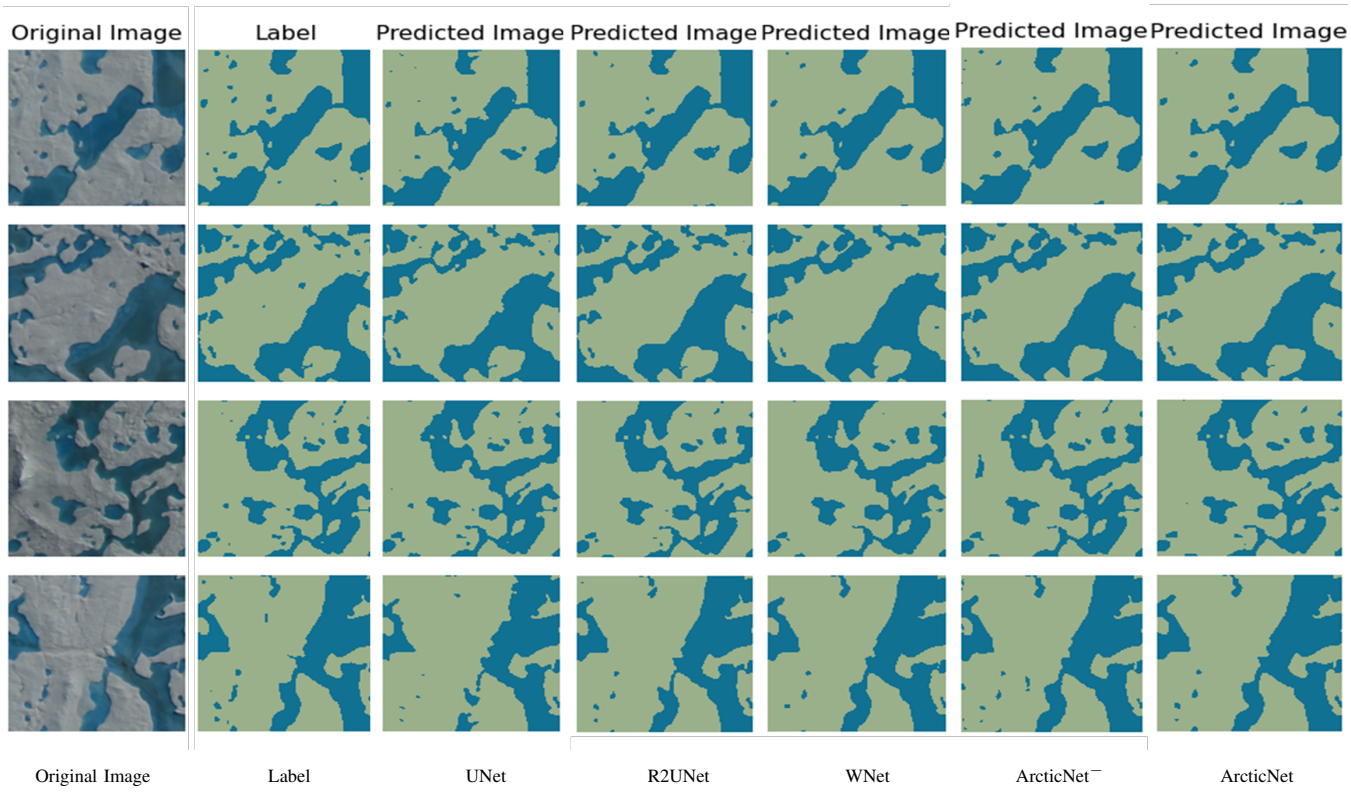

Fig. 7. Segmented outputs on NASA's Operation IceBridge dataset. Left to right: Original image, Label, and predicted segmentations by UNet, R2UNet, WNet, ArcticNet$^-$ and ArcticNet.
Legends: ■ Meltpond, ■ Snow.

TABLE III
QUANTITATIVE PERFORMANCE COMPARISON OF UNET, R2UNET, WNET, ARCTICNET$^-$ (ARCTICNET WITHOUT ATTENTION MECHANISM) AND ARCTICNET (WITH ATTENTION MECHANISM) EVALUATED ON OPERATION ICEBRIDGE DATASET.

	F1	ACC	PR	RE	mIOU
UNet	0.938	95.75%	0.969	0.914	0.885
R2UNet	0.956	96.95%	0.978	0.937	0.917
WNet	0.957	96.98%	0.973	0.943	0.918
ArcticNet$^-$	0.962	97.35%	0.976	0.950	0.928
ArcticNet	**0.969**	**97.85%**	**0.983**	**0.957**	**0.941**

D. Qualitative Analysis

Qualitative comparison of all the models is available in Fig. 6 and Fig. 7 for HOTRAX and Operation IceBridge datasets, respectively. The first, second, and the rest of the columns depict the original images, labels and predicted images of UNet, R2UNet, WNet, ArcticNet$^-$ and ArcticNet, respectively. In Fig. 6, the ground truth labels in rows 1, 3, and 4 exhibit slight boundary inconsistencies between meltpond, open water, and snow regions, where textural transitions are gradual rather than abrupt due to natural scene variability and surface ambiguities. The minor labeling uncertainties observed in some images are a consequence of subpixel mixing at these regions. ArcticNet's outputs within these regions align with visually plausible boundaries within this uncertainty margin, demonstrating improved sensitivity to subtle surface transitions. ArcticNet delineates the region boundaries efficiently compared to other models as shown in row 1 without focusing on the noise. Here, UNet, R2UNet and WNet misidentifies snow as a water channel. This indicates that ArcticNet can achieve higher boundary segmentation. For the qualitative comparison in Fig. 7, our model exhibits better performance in capturing the fine-grained details of sea ice and open water boundaries. However, even in the cases of correct predictions, misnomers in ground truthing will lead to an incorrect evaluation. In essence, ground truth errors may mislabel correct predictions as "incorrect," penalizing the model and reducing its perceived performance. The metrics defined in Table II and Table III may impede the model, suggesting poor segmentation results despite the model functioning at optimized capacity.

E. Cross-Validation

The model trained on the HOTRAX dataset (Sec. IV-B) was tested on the Operation IceBridge dataset, and the model trained on Operation IceBridge (Sec. IV-B) dataset was tested on the HOTRAX dataset. The evaluation focused primarily on the common classes, snow and meltponds. For consistency, the three-class model (snow, meltpond and openwater) was adapted by treating the third class, open water, as background and was merged with the snow (class 0).

Table IV summarizes the performance of three-class model trained on HOTRAX dataset and tested with the two-class Operation IceBridge dataset. Fig. 8 displays the segmented outputs of three-class model when evaluated on the two-class dataset.

Original Image Ground Truth Predicted Output

Fig. 8. Segmented outputs of three-class model trained on HOTRAX dataset and evaluated on two-class Operation IceBridge Dataset. Left: original image, center: ground truth, right: predicted output.
Legends: Meltpond, Snow.

Original Image Ground Truth Predicted Output

Fig. 9. Segmented outputs of two-class model trained on Operation IceBridge dataset and evaluated on three-class HOTRAX dataset. Left: original image, center: ground truth, right: predicted output.
Legends: Meltpond, Snow.

TABLE IV
QUANTITATIVE PERFORMANCE OF THREE-CLASS MODEL(TRAINED ON THE HOTRAX DATASET) ON THE TWO-CLASS DATASET(OPERATION ICEBRIDGE).

	Evaluation of three classes
Accuracy	96.51%
mIOU	0.8585

Table V summarizes the performance of the two-class model when applied to the three-class dataset. Fig. 9 displays the segmented output of the two-class model trained on the Operation IceBridge dataset and evaluated on the three-class HOTRAX dataset.

TABLE V
QUANTITATIVE PERFORMANCE OF TWO-CLASS MODEL(TRAINED ON THE OPERATION ICEBRIDGE DATASET) ON THE THREE-CLASS DATASET (HOTRAX).

	Evaluation of two classes
Accuracy	96.43%
mIOU	0.9602

F. Joint-Validation

All images from the HOTRAX and Operation IceBridge datasets were combined together to produce a joint model trained for both three-class and two-class settings. The training processes used a total of 180 images for training, 55 images for validation and 35 images for testing. Since the HOTRAX images have a resolution of $3042 \times 2048 \times 3$, they were randomly cropped to match the consistent size of the Operation IceBridge dataset, $1000 \times 1000 \times 3$. The model successfully detected the third class, open water, efficiently whenever it was present in the three-class setting. Table VI summarizes

TABLE VI
JOINT VALIDATION OF OPERATION ICEBRIDGE AND HOTRAX DATASET WHERE THE MODEL IS TRAINED FOR THREE CLASSES AND TWO CLASSES RESPECTIVELY.

	Evaluation of three classes on three-class model	Evaluation of two classes on two-class model
Accuracy	97.69%	97.55%
mIOU	0.9019	0.9520

Original Image (HOTRAX) Ground Truth Predicted Output

(a)

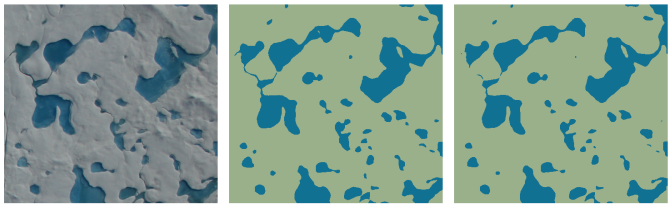

Original Image (Operation IceBridge) Ground Truth Predicted Output

(b)

Fig. 10. Segmented outputs of the model trained for three classes and evaluated on both (a) HOTRAX and (b) Operation IceBridge dataset. Left: original image, center: ground truth, right: predicted output.
Legends: Open water, Meltpond, Snow.

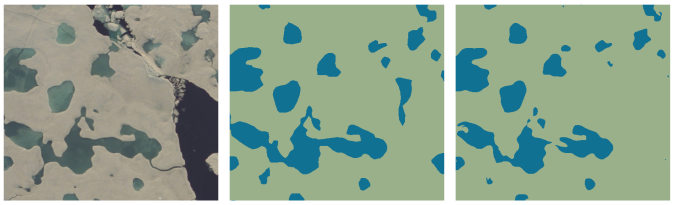

Original Image (HOTRAX) Ground Truth Predicted Output

(a)

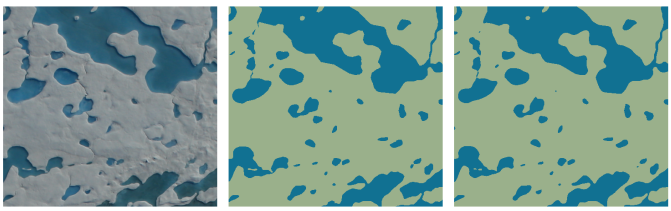

Original Image (Operation IceBridge) Ground Truth Predicted Output

(b)

Fig. 11. Segmented outputs of the model trained for two classes and evaluated on both (a) HOTRAX and (b) Operation IceBridge dataset. Left: original image, center: ground truth, right: predicted output.
Legends: Meltpond, Snow.

the joint validation of the HOTRAX and Operation IceBridge datasets trained as three classes, as well as two classes to evaluate the generic model performance.

Figures 10a and 10b represent the segmented output trained for three classes on both HOTRAX and Operation IceBridge datasets. Segmented outputs of the model trained for two classes and evaluated on the HOTRAX and Operation IceBridge datasets are shown in Figures 11a and 11b. The third class in the HOTRAX dataset was treated as class 0, representing the background (snow), so that the model could focus on common classes, such as meltponds and snow. This approach simplified the segmentation task and reduced the impact of less significant classes on the learning of the model.

V. Discussion

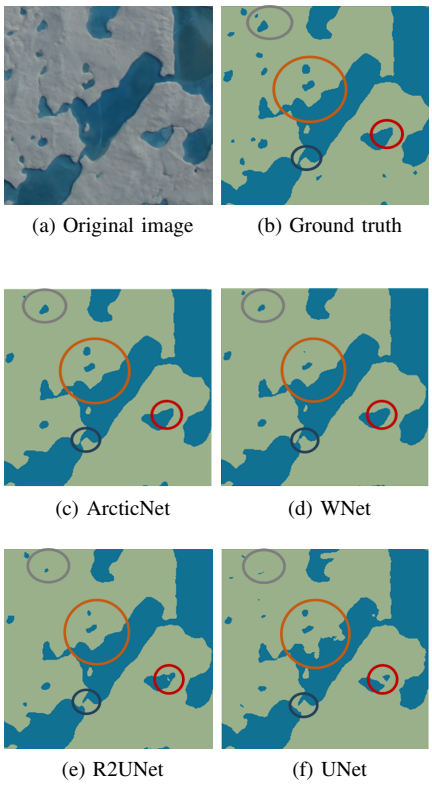

(a) Original image (b) Ground truth

(c) ArcticNet (d) WNet

(e) R2UNet (f) UNet

Fig. 12. Detailed observation of segmented regions produced by different architectures. (a) Original image (b) Ground truth (c) ArcticNet (d) WNet (e) R2UNet (f) UNet.
Legends: Meltpond, Snow.

In the quantitative analysis, ArcticNet shows superior results relative to the other models. Qualitative analysis corroborates this visually by focusing on meltpond boundaries. Figure 12 illustrates noticeable features with sharper and cleaner edges of meltponds. The black circle draws attention to the specific shortcomings of UNet, R2UNet and WNet in comparison with ArcticNet as ArcticNet picks up fine details observable in the ground truth image such as the thin curved boundary of the meltpond. Additionally, UNet and R2UNet are prone to true negative identifications as indicated by the red circles. Due to blurry or irregular meltpond boundaries, UNet and R2UNet struggle to sharply separate meltpond from surrounding ice, especially when transitions are gradual, which leads to incorrect non-meltpond labeling near true meltpond edges. Another point to note is that UNet and R2UNet perform aggressive downsampling to capture a larger context, potentially causing the loss of small-scale or thin structures such as narrow meltpond boundaries that are lost during feature extraction, causing under-detection of fine meltpond features. They also mainly use local receptive fields that may misinterpret complex textures or mixed surfaces such as thin ice vs shallow pond because they cannot model large-scale dependencies well. The unique challenge in meltpond segmentation is that meltponds are often thin, elongated and irregularly shaped with subtle intensity transitions relative to surrounding snow and ice. This requires a model that can preserve fine-scale boundary details while maintaining global context awareness to distinguish between very similar regions, and ArcticNet was specifically designed to meet these requirements. Meanwhile, WNet lacks the crisp boundaries associated with ArcticNet due to oversmoothing. WNet uses multi-branch feature fusion from deeper feature maps which can lead to over-smoothing during upsampling and reconstruction because features from different branches are blended together. Although WNet uses wide connections to preserve multiscale information, finer, pixel-level localization may still degrade during decoding. However, ArcticNet avoids oversmoothing during reconstruction by maintaining fine and coarse semantically rich details during the feature propagation from the decoder of the first UNet to the corresponding encoder of the second UNet resulting in shaper and cleaner boundaries. Another observation with true negatives is shown by orange and purple circles, reaffirming issues with true negatives and boundary clarity indicated in the red circles. While ArcticNet yields superior outcomes compared to UNet, R2UNet and WNet, including the demonstration of slightly better detection of smaller meltponds. Thus, attention mechanisms play major roles in capturing specific details that non-attention models might overlook, as they can better focus on global dependencies and detailed boundary information [63].

A. Impact of Attention Mechanism

The inclusion of the attention mechanism in ArcticNet significantly enhances the model's ability to focus on salient regions during segmentation, particularly around object boundaries. By weighting the importance of features, the attention gate selectively emphasizes regions that are critical for accurate segmentation, such as the foreground structures, while downplaying irrelevant background information. This selective focus allows the network to refine spatial details and improve boundary delineation, which is especially beneficial in complex or noisy scenes [40], [43]. This is particularly critical in disguising shallow meltponds from thin ice, which otherwise be misclassified as meltponds due to similar textures. By directing the focus of the model toward subtle boundary cues, the attention module reduces both boundary leakage and mislabeling of adjacent non-meltpond regions. As a result, ArcticNet achieves more precise segmentation outputs with improved foreground-background contrast, demonstrating the

crucial role of attention in guiding the network's learning toward the most informative features.

As such, we speculate that introducing an improved version of an attention gate may further improve the model's ability to generate sharp, clear boundaries that would otherwise have been missed. ArcticNet also demonstrates consistent improvements across metrics, including the F1 score, accuracy, precision, and recall, reflecting its robust feature representation and effectiveness in segmentation tasks. These consistent improvements highlight not only ArcticNet's architectural advantages but also its robustness and generalizability to varied snow-pond-open water patterns.

B. Impact of Skip Connection from Decoder of the first UNet to the Encoder of the Second UNet

Addition of the skip connection from the decoder of the first UNet to the encoder of the second UNet as in ArcticNet^{-} and ArcticNet introduces powerful enhancements to feature representation and segmentation accuracy. These connections allow the second UNet to receive semantically rich and context-aware features early in its encoding path, effectively initializing it with a higher-level understanding of the input. This facilitates more accurate and refined segmentation, particularly along object boundaries or in regions of ambiguity from the first prediction. This mechanism also improves feature propagation and gradient stability, mitigating the vanishing gradient problem seen in deeper stacked models [51]. It also allows the second UNet architecture to correct errors from the first stage by integrating both coarse context and fine details. This layered correction is particularly effective in refining ambiguous regions, such as partially frozen meltpond edges. The second UNet also benefits from the prior coarse segmentation as it integrates both low–level and high–level cues more effectively [44]. It learns to correct prior errors due to the availability of residual or corrective features from enriched input.

C. Limitations and Future Directions

Our analysis does not apply to special situations such as changes in meltpond extent due to coverage by fresh snowfall, or unusually high wind events. Fresh snowfall on ponds can cause temporary bright cover in the sea ice that removes the RGB contrast in the imagery and hides pond boundaries, leading to under-segmentation in the meltpond detection process. This could be mitigated by adding snow-overlay augmentations and exposure jitters on the captured data to flag low-confidence outputs [24]. Overnight skim-ice due to thin refreezing may lead to the formation of thin lids in the sea ice that could alter texture/brightness and blur region boundaries in the imagery leading to reduced performance in the detection process. Focusing on the boundary-aware losses and training with skim like textures may improve the detection results in this scenario [64]. Illumination extremes in the Arctic region may cause strong shadows and glints, and saturation may lead to the degradation of the boundary quality in the imagery causing model under-performance. Introducing photometric normalization [65] in the preprocessing stage and test-time augmentation in the post-processing may mitigate this issue [66]. Model performance may be affected by out-of-distribution scenes due to sensor characteristics, season changes, and ice-type variations. This could be mitigated through the application of advanced methodologies for domain adaptation/expansion [67], [68], self-training [69], [70], and uncertainty-driven triage [71], [72].

VI. Conclusion

We presented a deep CNN network namely, ArcticNet which is based on the fundamental principles of UNet, R2UNet and WNet for the localization of meltponds in Arctic seas. The effectiveness of the model was evaluated with HOTRAX and Operation IceBridge imagery datasets for pixel-level multi-class classification and extraction of boundaries of meltponds on the Arctic sea surface. ArcticNet outperformed other deep learning architectures (UNet, R2UNet and WNet) due to an increased model capacity. The feature propagation phenomenon in the proposed model that helped the transmission of high-level features from the decoding units of the first UNet to the encoding units of the second UNet in a hierarchical manner benefited during the segmentation task. Incorporation of the residual and recurrent operations in the architecture broadened the scope of segmentation by offering a more comprehensive view and accumulation of low-level features. Integration of attention gates in the ArcticNet helped in focusing of target areas of various shapes and sizes which enhanced its overall performance and reliability. This addition boosted the model sensitivity and refined predictions which contributed to a greater robustness of the network.

The improved segmentation accuracy achieved by ArcticNet, compared to earlier architectures, can significantly enhance subsequent research on meltpond changes. More accurate delineation of the boundaries of the meltpond will lead to more reliable estimates of meltpond area, distribution, and evolution, which are critical indicators in the Arctic and the progression of climate change. Enhanced segmentation reduces the propagation of measurement errors in downstream analyses, such as modeling surface albedo, predicting ice melt rates, and forecasting Arctic climate feedback mechanisms. Furthermore, improved accuracy ensures that even small or fragmented meltponds are better detected, allowing researchers to capture early-stage pond formation and subtle morphological variations that were previously overlooked, and also support better-informed policy decisions regarding climate change mitigation. Thus, ArcticNet's improved performance is not just a technical advancement, but a crucial enabler for deeper, more precise environmental insights.

Acknowledgments

This work is supported by the Division of Physics at the U.S. National Science Foundation (NSF), Grant No. 2102906.

The authors would like to thank Shaik Nordin Abouzahra and Dr. Theus Aspiras for their insight and assistance throughout this work. The authors would like to extend their gratitude to Kassam Madmouj and Jordan Powell for their role in helping label the Operation IceBridge dataset.

REFERENCES

[1] A. Sultana, V. K. Asari, T. Aspiras, R. Liu, I. Sudakow, and L. W. Cooper, "NABLA-n for meltpond detection," in *Pattern Recognition and Prediction XXXV*, M. S. Alam and V. K. Asari, Eds., Backup Publisher: International Society for Optics and Photonics, vol. 13040, SPIE, 2024, p. 1 304 006. DOI: 10.1117/12.3016570. [Online]. Available: https://doi.org/10.1117/12.3016570.

[2] S. Aparício, "Review article: Earth observations of melt ponds on sea ice," *The Cryosphere Discussions*, vol. 2023, pp. 1–65, 2023. DOI: 10.5194/tc-2023-75. [Online]. Available: https://tc.copernicus.org/preprints/tc-2023-75/.

[3] D. K. Perovich and W. B. Tucker, "Arctic sea-ice conditions and the distribution of solar radiation during summer," *Annals of Glaciology*, vol. 25, pp. 445–450, 1997. DOI: 10.3189/S0260305500014439.

[4] J. Stroeve and D. Notz, "Changing state of arctic sea ice across all seasons," *Environmental Research Letters*, vol. 13, no. 10, p. 103 001, Sep. 2018, Publisher: IOP Publishing. DOI: 10.1088/1748-9326/aade56. [Online]. Available: https://dx.doi.org/10.1088/1748-9326/aade56.

[5] J. A. Curry, J. L. Schramm, and E. E. Ebert, "Sea ice-albedo climate feedback mechanism," *Journal of Climate*, vol. 8, no. 2, pp. 240–247, 1995, Place: Boston MA, USA Publisher: American Meteorological Society. DOI: 10.1175/1520-0442(1995)008⟨0240:SIACFM⟩2.0.CO;2. [Online]. Available: https://journals.ametsoc.org/view/journals/clim/8/2/1520-0442_1995_008_0240_siacfm_2_0_co_2.xml.

[6] A. Sultana et al., "Diffusion model-based generation of sea ice data," in *Multimodal Image Exploitation and Learning 2024*, S. S. Agaian, V. K. Asari, and S. P. DelMarco, Eds., Backup Publisher: International Society for Optics and Photonics, vol. 13033, SPIE, 2024, 130330B. DOI: 10.1117/12.3016574. [Online]. Available: https://doi.org/10.1117/12.3016574.

[7] N. Panchi, E. Kim, and A. Bhattacharyya, "Supplementing remote sensing of ice: Deep learning-based image segmentation system for automatic detection and localization of sea-ice formations from close-range optical images," *IEEE Sensors Journal*, vol. PP, pp. 1–1, May 2021. DOI: 10.1109/JSEN.2021.3084556.

[8] Q. Zhang, R. Skjetne, and B. Su, "Automatic image segmentation for boundary detection of apparently connected sea-ice floes," Jun. 2013.

[9] L.-K. Soh and C. Tsatsoulis, "Automated sea ice segmentation (ASIS)," in *IGARSS '98. Sensing and Managing the Environment. 1998 IEEE International Geoscience and Remote Sensing. Symposium Proceedings. (Cat. No.98CH36174)*, vol. 2, 1998, 586–588 vol.2. DOI: 10.1109/IGARSS.1998.699519.

[10] J. Kaur, S. Agrawal, and V. Renu, "A comparative analysis of thresholding and edge detection segmentation techniques," *International Journal of Computer Applications*, vol. 39, pp. 29–34, Feb. 2012. DOI: 10.5120/4898-7432.

[11] D. Haverkamp, L. Soh, and C. Tsatsoulis, "A dynamic local thresholding technique for sea ice classification," in *Proceedings of IGARSS '93 - IEEE International Geoscience and Remote Sensing Symposium*, 1993, 638–640 vol.2. DOI: 10.1109/IGARSS.1993.322252.

[12] I. Sudakow, V. K. Asari, R. Liu, and D. Demchev, "MeltPondNet: A swin transformer u-net for detection of melt ponds on arctic sea ice," *IEEE Journal of Selected Topics in Applied Earth Observations and Remote Sensing*, vol. 15, pp. 8776–8784, 2022. DOI: 10.1109/JSTARS.2022.3213192.

[13] S. Kern, A. Rösel, L. Pedersen, N. Ivanova, R. Saldo, and R. Tonboe, "The impact of melt ponds on summertime microwave brightness temperatures and sea-ice concentrations," English, *The Cryosphere*, vol. 10, no. 5, pp. 2217–2239, 2016, ISSN: 1994-0416. DOI: 10.5194/tc-10-2217-2016.

[14] *What is the cryosphere?* Publication Title: National Snow and Ice Data Center. Accessed: Aug. 9, 2024. [Online]. Available: https://nsidc.org/learn/what-cryosphere.

[15] D. K. Perovich and C. Polashenski, "Albedo evolution of seasonal arctic sea ice," *Geophysical Research Letters*, vol. 39, no. 8, 2012. DOI: https://doi.org/10.1029/2012GL051432. [Online]. Available: https://agupubs.onlinelibrary.wiley.com/doi/abs/10.1029/2012GL051432.

[16] B. Light, T. C. Grenfell, and D. K. Perovich, "Transmission and absorption of solar radiation by arctic sea ice during the melt season," *Journal of Geophysical Research: Oceans*, vol. 113, no. C3, 2008. DOI: https://doi.org/10.1029/2006JC003977. [Online]. Available: https://agupubs.onlinelibrary.wiley.com/doi/abs/10.1029/2006JC003977.

[17] D. K. Perovich, T. C. Grenfell, Transmission, B. absorption of solar radiation, and P. V. Hobbs, "Seasonal evolution of the albedo of multiyear arctic sea ice," *Journal of Geophysical Research: Oceans*, vol. 107, no. C10, SHE 20-1-SHE 20–13, 2002. DOI: https://doi.org/10.1029/2000JC000438. [Online]. Available: https://agupubs.onlinelibrary.wiley.com/doi/abs/10.1029/2000JC000438.

[18] M. Lüthje, D. L. Feltham, P. D. Taylor, and M. G. Worster, "Modeling the summertime evolution of sea-ice melt ponds," *Journal of Geophysical Research: Oceans*, vol. 111, no. C2, 2006. DOI: https://doi.org/10.1029/2004JC002818. [Online]. Available: https://agupubs.onlinelibrary.wiley.com/doi/abs/10.1029/2004JC002818.

[19] M. A. Webster, I. G. Rigor, D. K. Perovich, J. A. Richter-Menge, C. M. Polashenski, and B. Light, "Seasonal evolution of melt ponds on arctic sea ice," *Journal of Geophysical Research: Oceans*, vol. 120, no. 9, pp. 5968–5982, 2015. DOI: https://doi.org/10.1002/2015JC011030. [Online]. Available: https://

agupubs.onlinelibrary.wiley.com/doi/abs/10.1002/2015JC011030.

[20] F. Scott and D. L. Feltham, "A model of the three-dimensional evolution of arctic melt ponds on first-year and multiyear sea ice," *Journal of Geophysical Research: Oceans*, vol. 115, no. C12, 2010. DOI: https://doi.org/10.1029/2010JC006156. [Online]. Available: https://agupubs.onlinelibrary.wiley.com/doi/abs/10.1029/2010JC006156.

[21] Y. Liang, H. Bi, X. Chen, Y. Chen, and X. Wang, "The pacific arctic region has become a sink for multiyear sea ice coverage," *Geophysical Research Letters*, vol. 52, no. 16, e2025GL117093, 2025. DOI: https://doi.org/10.1029/2025GL117093. [Online]. Available: https://agupubs.onlinelibrary.wiley.com/doi/abs/10.1029/2025GL117093.

[22] M. Nicolaus, C. Katlein, J. Maslanik, and S. Hendricks, "Changes in arctic sea ice result in increasing transmission and absorption of solar radiati transmittance and absorption," *Geophysical Research Letters*, vol. 39, no. 24, 2012. DOI: https://doi.org/10.1029/2012GL053738. [Online]. Available: https://agupubs.onlinelibrary.wiley.com/doi/abs/10.1029/2012GL053738.

[23] B. Light et al., "Arctic sea ice albedo: Spectral composition, spatial heterogeneity, and temporal evolution observed during the mosaic drift," *Elementa: Science of the Anthropocene*, vol. 10, no. 1, p. 000 103, Aug. 2022, ISSN: 2325-1026. DOI: 10.1525/elementa.2021.000103. [Online]. Available: https://doi.org/10.1525/elementa.2021.000103.

[24] P. Anhaus, C. Katlein, M. Nicolaus, M. Hoppmann, and C. Haas, "From bright windows to dark spots: Snow cover controls melt pond optical properties during refreezing," *Geophysical Research Letters*, vol. 48, no. 23, e2021GL095369, 2021. DOI: https://doi.org/10.1029/2021GL095369. [Online]. Available: https://agupubs.onlinelibrary.wiley.com/doi/abs/10.1029/2021GL095369.

[25] A. Rösel, L. Kaleschke, and G. Birnbaum, "Melt ponds on arctic sea ice determined from modis satellite data using an artificial neural network," *The Cryosphere*, vol. 6, no. 2, pp. 431–446, 2012. DOI: 10.5194/tc-6-431-2012. [Online]. Available: https://tc.copernicus.org/articles/6/431/2012/.

[26] E. Zege et al., "Algorithm to retrieve the melt pond fraction and the spectral albedo of arctic summer ice from satellite optical data," *Remote Sensing of Environment*, vol. 163, pp. 153–164, 2015, ISSN: 0034-4257. DOI: https://doi.org/10.1016/j.rse.2015.03.012. [Online]. Available: https://www.sciencedirect.com/science/article/pii/S003442571500108X.

[27] J. J. Yackel and D. G. Barber, "Melt ponds on sea ice in the canadian archipelago: 2. on the use of radarsat-1 synthetic aperture radar for geophysical inversion," *Journal of Geophysical Research: Oceans*, vol. 105, no. C9, pp. 22 061–22 070, 2000. DOI: https://doi.org/10.1029/2000JC900076. [Online]. Available: https://agupubs.onlinelibrary.wiley.com/doi/abs/10.1029/2000JC900076.

[28] A. S. Fors, D. V. Divine, A. P. Doulgeris, A. H. H. Renner, and S. Gerland, "Signature of arctic first-year ice melt pond fraction in x-band sar imagery," *The Cryosphere*, vol. 11, no. 2, pp. 755–771, 2017. DOI: 10.5194/tc-11-755-2017. [Online]. Available: https://tc.copernicus.org/articles/11/755/2017/.

[29] H. Han et al., "Retrieval of melt ponds on arctic multi-year sea ice in summer from terrasar-x dual-polarization data using machine learning approaches: A case study in the chukchi sea with mid-incidence angle data," *Remote. Sens.*, vol. 8, p. 57, 2016. [Online]. Available: https://api.semanticscholar.org/CorpusID:2985926.

[30] M. Barjatia, T. Tasdizen, B. Song, C. Sampson, and K. M. Golden, "Network modeling of arctic melt ponds," *Cold Regions Science and Technology*, vol. 124, pp. 40–53, 2016, ISSN: 0165-232X. DOI: https://doi.org/10.1016/j.coldregions.2015.11.019. [Online]. Available: https://www.sciencedirect.com/science/article/pii/S0165232X15002992.

[31] C. Derksen, J. Piwowar, and E. LeDrew, "Sea-ice melt-pond fraction as determined from low level aerial photographs," *Arctic and Alpine Research*, vol. 29, no. 3, pp. 345–351, 1997, ISSN: 00040851. Accessed: Jan. 13, 2025. [Online]. Available: http://www.jstor.org/stable/1552150.

[32] M. Mäkynen, S. Kern, A. Rösel, and L. T. Pedersen, "On the estimation of melt pond fraction on the arctic sea ice with envisat wsm images," *IEEE Transactions on Geoscience and Remote Sensing*, vol. 52, no. 11, pp. 7366–7379, 2014. DOI: 10.1109/TGRS.2014.2311476.

[33] D. Kim, B. Hwang, K. Chung, S. Lee, H. Jung, and W. Moon, "Melt pond mapping with high-resolution sar: The first view," English, *Proceedings of the IEEE*, vol. 101, no. 3, pp. 748–758, Jan. 2013, ISSN: 0018-9219. DOI: 10.1109/JPROC.2012.2226411.

[34] L. Li, C. Ke, H. Xie, R. Lei, and A. Tao, "Aerial observations of sea ice and melt ponds near the North Pole during CHINARE2010," *Acta Oceanologica Sinica*, vol. 36, no. 1, pp. 64–72, Jan. 2017. DOI: 10.1007/s13131-017-0994-2.

[35] S. Lee, J. Stroeve, M. Tsamados, and A. L. Khan, "Machine learning approaches to retrieve pan-arctic melt ponds from visible satellite imagery," *Remote Sensing of Environment*, vol. 247, p. 111 919, 2020, ISSN: 0034-4257. DOI: https://doi.org/10.1016/j.rse.2020.111919. [Online]. Available: https://www.sciencedirect.com/science/article/pii/S0034425720302893.

[36] O. Ronneberger, P. Fischer, and T. Brox, *U-net: Convolutional networks for biomedical image segmentation*, _eprint: 1505.04597, 2015. [Online]. Available: https://arxiv.org/abs/1505.04597.

[37] L.-C. Chen, G. Papandreou, I. Kokkinos, K. Murphy, and A. L. Yuille, *DeepLab: Semantic image segmentation with deep convolutional nets, atrous convolution,*

and fully connected CRFs, _eprint: 1606.00915, 2017. [Online]. Available: https://arxiv.org/abs/1606.00915.

[38] H. Zhao, J. Shi, X. Qi, X. Wang, and J. Jia, *Pyramid scene parsing network*, _eprint: 1612.01105, 2017. [Online]. Available: https://arxiv.org/abs/1612.01105.

[39] X. Xia and B. Kulis, *W-net: A deep model for fully unsupervised image segmentation*, _eprint: 1711.08506, 2017. [Online]. Available: https://arxiv.org/abs/1711.08506.

[40] O. Oktay et al., *Attention u-net: Learning where to look for the pancreas*, _eprint: 1804.03999, 2018. [Online]. Available: https://arxiv.org/abs/1804.03999.

[41] M. Z. Alom, M. Hasan, C. Yakopcic, T. M. Taha, and V. K. Asari, *Recurrent residual convolutional neural network based on u-net (r2u-net) for medical image segmentation*, _eprint: 1802.06955, 2018. [Online]. Available: https://arxiv.org/abs/1802.06955.

[42] M. Tan and Q. V. Le, *EfficientNet: Rethinking model scaling for convolutional neural networks*, _eprint: 1905.11946, 2020. [Online]. Available: https://arxiv.org/abs/1905.11946.

[43] Q. Zuo, S. Chen, and Z. Wang, "R2au-net: Attention recurrent residual convolutional neural network for multimodal medical image segmentation," *Security and Communication Networks*, vol. 2021, no. 1, p. 6 625 688, 2021, _eprint: https://onlinelibrary.wiley.com/doi/pdf/10.1155/2021/6625688. DOI: https://doi.org/10.1155/2021/6625688. [Online]. Available: https://onlinelibrary.wiley.com/doi/abs/10.1155/2021/6625688.

[44] C. Wang, X. Jiang, Z. Wang, X. Guo, W. Wan, and J. Wang, "AMB-wnet: Embedding attention model in multi-bridge wnet for exploring the mechanics of disease," *Gene Expression Patterns*, vol. 45, p. 119 259, 2022, ISSN: 1567-133X. DOI: https://doi.org/10.1016/j.gep.2022.119259. [Online]. Available: https://www.sciencedirect.com/science/article/pii/S1567133X22000291.

[45] M. Gargiulo, D. A. G. Dell'Aglio, A. Iodice, D. Riccio, and G. Ruello, "Integration of sentinel-1 and sentinel-2 data for land cover mapping using w-net," *Sensors*, vol. 20, no. 10, 2020, ISSN: 1424-8220. DOI: 10.3390/s20102969. [Online]. Available: https://www.mdpi.com/1424-8220/20/10/2969.

[46] A. Sultana, V. K. Asari, I. Sudakow, T. Aspiras, R. Liu, and D. Demchev, "R2unet for melt pond detection," in *Pattern Recognition and Tracking XXXIV*, M. S. Alam and V. K. Asari, Eds., Backup Publisher: International Society for Optics and Photonics, vol. 12527, SPIE, 2023, 125270R. DOI: 10.1117/12.2663982. [Online]. Available: https://doi.org/10.1117/12.2663982.

[47] A. Sherstinsky, "Fundamentals of recurrent neural network (RNN) and long short-term memory (LSTM) network," *CoRR*, vol. abs/1808.03314, 2018. arXiv: 1808.03314. [Online]. Available: http://arxiv.org/abs/1808.03314.

[48] Y. Bengio, P. Frasconi, and P. Y. Simard, "The problem of learning long-term dependencies in recurrent networks," *IEEE International Conference on Neural Networks*, 1183–1188 vol.3, 1993. [Online]. Available: https://api.semanticscholar.org/CorpusID:61166081.

[49] R. Pascanu, T. Mikolov, and Y. Bengio, "On the difficulty of training recurrent neural networks," *30th International Conference on Machine Learning, ICML 2013*, Nov. 2012.

[50] K. He, X. Zhang, S. Ren, and J. Sun, *Deep residual learning for image recognition*, _eprint: 1512.03385, 2015. [Online]. Available: https://arxiv.org/abs/1512.03385.

[51] Z. Zhang, Q. Liu, and Y. Wang, "Road extraction by deep residual u-net," *IEEE Geoscience and Remote Sensing Letters*, vol. 15, no. 5, pp. 749–753, May 2018, Publisher: Institute of Electrical and Electronics Engineers (IEEE), ISSN: 1558-0571. DOI: 10.1109/lgrs.2018.2802944. [Online]. Available: http://dx.doi.org/10.1109/LGRS.2018.2802944.

[52] A. Sultana, "Residues in succession u-net for fast and efficient segmentation," Ph.D. dissertation, University of Dayton, 2022. [Online]. Available: http://rave.ohiolink.edu/etdc/view?acc_num=dayton1659016279233472.

[53] A. Sultana, V. K. Asari, and T. Aspiras, "Residues in succession recurrent u-net for segmentation of retinal blood vessels," in *Pattern Recognition and Tracking XXXIV*, M. S. Alam and V. K. Asari, Eds., Backup Publisher: International Society for Optics and Photonics, vol. 12527, SPIE, 2023, p. 1 252 706. DOI: 10.1117/12.2664876. [Online]. Available: https://doi.org/10.1117/12.2664876.

[54] J. Schlemper et al., "Attention gated networks: Learning to leverage salient regions in medical images," *Medical Image Analysis*, vol. 53, pp. 197–207, 2019, ISSN: 1361-8415. DOI: https://doi.org/10.1016/j.media.2019.01.012. [Online]. Available: https://www.sciencedirect.com/science/article/pii/S1361841518306133.

[55] *TensorFlow*, Publication Title: TensorFlow. Accessed: Aug. 9, 2024. [Online]. Available: https://www.tensorflow.org/.

[56] *Keras: Deep learning for humans*. Accessed: Aug. 9, 2024. [Online]. Available: https://keras.io/.

[57] *Polar Science Center; HOTRAX — psc.apl.uw.edu*, https://psc.apl.uw.edu/?s=HOTRAX, [Accessed 03-12-2024].

[58] D. A. Darby, L. Polyak, and M. Jakobsson, "The 2005 hotrax expedition to the arctic ocean," *Global and Planetary Change*, vol. 68, no. 1, pp. 1–4, 2009, ISSN: 0921-8181. DOI: https://doi.org/10.1016/j.gloplacha.2009.04.005. [Online]. Available: https://www.sciencedirect.com/science/article/pii/S0921818109000952.

[59] A. Sultana, V. Asari, I. Sudakow, R. Liu, and D. Demchev, *Melt pond UNet for the segmentation of the Arctic area, Aug-Sept 2005*, en, 2022. DOI: 10.18739/A20G3H067. Accessed: Aug. 9, 2024. [Online]. Available: https://arcticdata.io/catalog/view/doi:10.18739/A20G3H067.

[60] I. Sudakow, V. Asari, R. Liu, and D. Demchev, "Melt pond from aerial photographs of the healy–oden trans

arctic expedition (HOTRAX)," Jun. 2022, Publisher: Zenodo Version Number: 1.0. DOI: 10.5281/zenodo.6602409. [Online]. Available: https://doi.org/10.5281/zenodo.6602409.

[61] A. Sultana, V. K. Asari, I. Sudakow, and L. W. Cooper, "Arcticnet: Meltpond region localization in the arctic," Jan. 2025. DOI: 10.36227/techrxiv.173835285.58180903/v1. [Online]. Available: http://dx.doi.org/10.36227/techrxiv.173835285.58180903/v1.

[62] R. Dominguez, *IceBridge DMS l1b geolocated and orthorectified images, version 1*, 2010. DOI: 10.5067/OZ6VNOPMPRJ0. [Online]. Available: https://nsidc.org/data/IODMS1B/versions/1.

[63] L. Huang, W. Wang, J. Chen, and X.-Y. Wei, *Attention on attention for image captioning*, _eprint: 1908.06954, 2019. [Online]. Available: https://arxiv.org/abs/1908.06954.

[64] D. Flocco, D. L. Feltham, E. Bailey, and D. Schroeder, "The refreezing of melt ponds on arctic sea ice," *Journal of Geophysical Research: Oceans*, vol. 120, no. 2, pp. 647–659, 2015. DOI: https://doi.org/10.1002/2014JC010140. [Online]. Available: https://agupubs.onlinelibrary.wiley.com/doi/abs/10.1002/2014JC010140.

[65] V. Štruc and N. Pavesic, "Photometric normalization techniques for illumination invariance," in Jan. 2011, pp. 279–300.

[66] M. Kimura, *Understanding test-time augmentation*, 2024. arXiv: 2402.06892 [cs.LG]. [Online]. Available: https://arxiv.org/abs/2402.06892.

[67] H. Liu, J. Wang, and M. Long, "Cycle self-training for domain adaptation," *CoRR*, vol. abs/2103.03571, 2021. arXiv: 2103.03571. [Online]. Available: https://arxiv.org/abs/2103.03571.

[68] L. Li et al., *Progressive domain expansion network for single domain generalization*, 2021. arXiv: 2103.16050 [cs.CV]. [Online]. Available: https://arxiv.org/abs/2103.16050.

[69] B. Zoph et al., *Rethinking pre-training and self-training*, 2020. arXiv: 2006.06882 [cs.CV]. [Online]. Available: https://arxiv.org/abs/2006.06882.

[70] M.-R. Amini, V. Feofanov, L. Pauletto, L. Hadjadj, É. Devijver, and Y. Maximov, "Self-training: A survey," *Neurocomputing*, vol. 616, p. 128 904, Feb. 2025, ISSN: 0925-2312. DOI: 10.1016/j.neucom.2024.128904. [Online]. Available: http://dx.doi.org/10.1016/j.neucom.2024.128904.

[71] Z. Luo, X. Luo, Z. Gao, and G. Wang, *An uncertainty-guided tiered self-training framework for active source-free domain adaptation in prostate segmentation*, 2024. arXiv: 2407.02893 [cs.CV]. [Online]. Available: https://arxiv.org/abs/2407.02893.

[72] X. Li et al., *At-cxr: Uncertainty-aware agentic triage for chest x-rays*, 2025. arXiv: 2508.19322 [eess.IV]. [Online]. Available: https://arxiv.org/abs/2508.19322.

VII. Biography Section

Aqsa Sultana (Student Member, IEEE) has a Master's degree in Computer Engineering and is currently pursuing her PhD in Electrical Engineering at the University of Dayton. Her research interests encompass remote sensing applications, neuromorphic computing/spiking neural networks, automated feature extraction and pattern recognition algorithms for oncology.

Vijayan K. Asari (Senior Member, IEEE) received the Ph.D. degree in electrical engineering from the Indian Institute of Technology Madras, Chennai, India, in 1994. He is currently a Professor of Electrical and Computer Engineering and the Ohio Research Scholars Endowed Chair in wide area surveillance with the University of Dayton, Dayton, OH, USA, where he is also the Director of the Center of Excellence for Computational Intelligence and Machine Vision (Vision Lab). He holds five U.S. patents and has authored or coauthored more than 700 research articles, including an edited book in wide area surveillance and 140 peer-reviewed journal papers in the areas of image processing, pattern recognition, machine learning, deep learning, and artificial neural networks. Professor Asari is a Senior Member of IEEE and an elected Fellow of SPIE, and a Co-Organizer of several SPIE and IEEE conferences and workshops. He is a recipient of several teaching, research, advising, and technical leadership awards, including the University of Dayton School of Engineering Vision Award for Excellence in August 2017, the Outstanding Engineers and Scientists Award for Technical Leadership from The Affiliate Societies Council of Dayton in April 2015, and the Sigma Xi George B. Noland Award for Outstanding Research in April 2016.

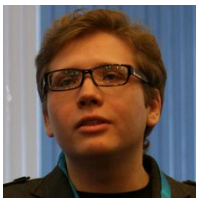

Ivan Sudakow (Senior Member, IEEE) received the master's degree in physics from Ural State University, Ekaterinburg, Russia, in 2008, and the Ph.D. degree in applied mathematics from Novgorod State University, Veliky Novgorod, Russia, in 2012. He has been an Assistant Professor with the Department of Physics, University of Dayton, for a long time. He is currently a Lecturer of Applied Mathematics with the School of Mathematics and Statistics, The Open University, Milton Keynes, U.K. He is also a Scholar with the SETI Institute, Mountain View, CA, USA. He specializes in data analysis and mathematical modeling for physical and living systems. Dr. Sudakow was awarded by German Federal Government the title "Green Talent" in 2013 for "his outstanding research of sea ice and his strong commitment to interdisciplinary interaction between mathematics and climate science".

Lee Cooper received the Ph.D. degree from the University of Alaska Fairbanks in 1987 and a M.S. degree from the University of Washington in 1980. He is currently a Professor at the Chesapeake Biological Laboratory, a unit of the University of Maryland Center for Environmental Science. He has served as chair of the Arctic Icebreaker Coordinating Committee of the University National Oceanographic Laboratory System, and as chair of the Marine Working Group of International Arctic Science Committee. He is the section editor for Biogeochemistry for the open science journal PLOS ONE. He primarily works on scientific questions involving biogeochemical processes in Arctic marine systems, including the biological and biogeochemical impacts of reduced sea ice cover in the Arctic Ocean.